Magnetic properties of ordered perovskites Ba_2LnTaO_6 (Ln = Y, lanthanides)

2001 J. Phys.: Condens. Matter 13 4191

(http://iopscience.iop.org/0953-8984/13/19/302)

INSTITUTE OF PHYSICS PUBLISHING JOURNAL OF PHYSICS: CONDENSED MATTER

J. Phys.: Condens. Matter **13** (2001) 4191–4202 www.iop.org/Journals/cm PII: S0953-8984(01)21582-3

Magnetic properties of ordered perovskites Ba_2LnTaO_6 (Ln = Y, lanthanides)

Yoshihiro Doi and Yukio Hinatsu

Division of Chemistry, Graduate School of Science, Hokkaido University, Sapporo 060-0810, Japan

Received 1 February 2001, in final form 21 March 2001

Abstract

Magnetic properties of the quaternary oxides Ba_2LnTaO_6 (Ln = Y or lanthanides) are reported. Their powder x-ray diffraction measurements and Rietveld analysis show that they have an ordered perovskite structure and are monoclinic (Ln = La–Tb) with space group $P2_1/n$ or cubic (Ln = Y, Dy–Lu) with space group $Fm\bar{3}m$. Magnetic susceptibilities of Ba_2LnTaO_6 were measured. All compounds in this work are paramagnetic down to 5 K. Ba_2EuTaO_6 and Ba_2SmTaO_6 show Van Vleck paramagnetism; their spin-orbit coupling constants are determined to be 331 cm^{-1} and 287 cm^{-1}, respectively. ^{151}Eu Mössbauer measurements for Ba_2EuTaO_6 were carried out at 12, 100, 200 and 300 K. The Eu ion is in the trivalent state, and the symmetry of the Eu site is distorted from the octahedral symmetry. The Debye temperature of Eu^{3+} was determined to be 335 K from the temperature dependence of the absorption area of intensity curves.

1. Introduction

The perovskite-type oxides have the general formula ABO_3, in which A represents a large transition metal ion and B represents a small one. It is known that the B site can accommodate two kinds of metal ion. The general formula of such a system is given as $A_2B'B''O_6$. Depending on the valences and relative ionic radii of all the ions involved, the B′ and B″ ions are settled with either random or ordered arrangement as investigated for many systems so far [1–4]. Since the B cations generally determine the physical properties of perovskites, the different kinds of B′ and B″ ion should show a variety of physical properties of ordered perovskites.

A series of the perovskites, Ba_2LnTaO_6 (Ln = Y or lanthanide elements), has an ordered arrangement of the Ln and Ta ions [5, 6]. According to Galasso *et al* [6], these compounds have an orthorhombic unit cell (for a La compound) a tetragonal cell (for a Gd compound) and cubic cells (for Y, Dy–Lu compounds). Recently, Taira *et al* reported the magnetic susceptibilities of Ba_2YbTaO_6 and the EPR spectrum of Yb^{3+} doped in Ba_2LuTaO_6 [7]. They determined the energy level of the ground state and two excited states for the Yb^{3+} ion, and suggested the existence of covalency in the Yb^{3+} ion in the octahedral symmetry. The valences of the Ln and Ta ions in Ba_2LnTaO_6 are 3+ ($[Xe]4f^n$) and 5+ ($[Xe]4f^{14}5d^0$), respectively ([Xe]: electronic xenon core). Only Ln^{3+} ions contribute to the magnetic behaviour of this series of

0953-8984/01/194191+12$30.00

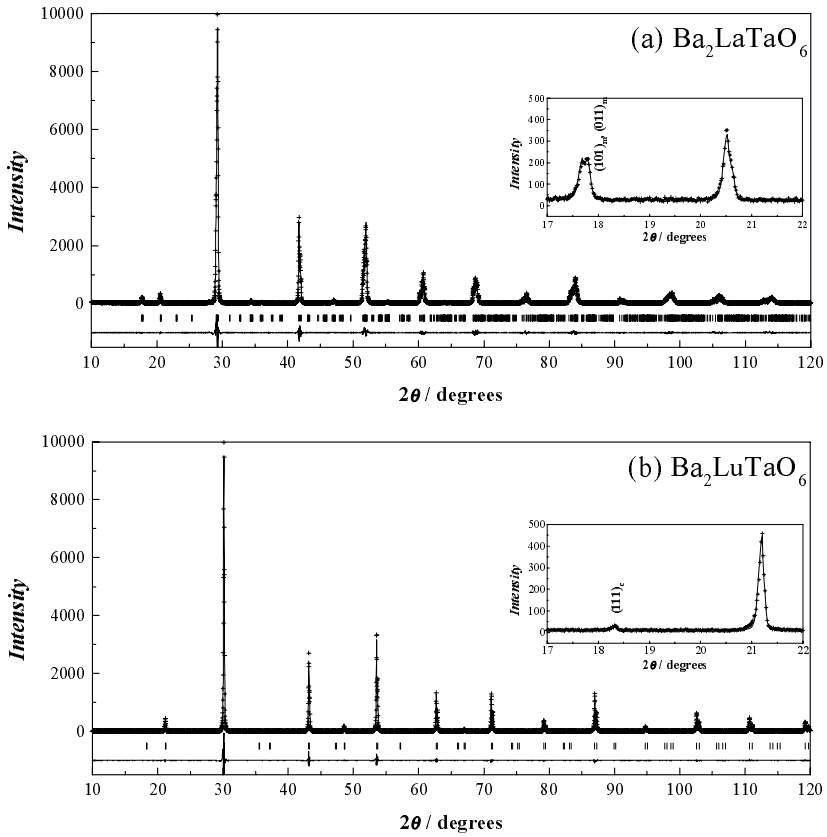

Figure 1. X-ray diffraction profiles for Ba_2LaTaO_6 (a) and Ba_2LuTaO_6 (b). The calculated and observed diffraction profiles are shown on the top solid line and cross markers, respectively. The vertical marks in the middle show positions calculated from Bragg reflections. The bottom trace is a plot of the difference between calculated and observed intensities. The insets show the enlargement of the profiles at low angle.

compounds (i.e. Ta^{5+} ion is nonmagnetic). Therefore, this system is appropriate for the study of the magnetic properties of f electrons in the B sites of ordered perovskites.

In this work, we will report the structural and magnetic properties of Ba_2LnTaO_6 (Ln = Y or lanthanides) in detail. The crystal structures at room temperature were refined by the Rietveld analysis of the powder x-ray diffraction data. Their magnetic susceptibility measurements were performed in the temperature range between 5 and 300 K. In addition, ^{151}Eu Mössbauer spectra for Ba_2EuTaO_6 were measured at 12, 100, 200 and 300 K.

2. Experiment

A series of Ba_2LnTaO_6 compounds was synthesized by the solid-state reaction method. Starting materials were $BaCO_3$, Ln_2O_3 (Ln = Y, La, Nd, Sm–Gd, Dy–Lu), Pr_6O_{11}, Tb_4O_7 and Ta_2O_5. These reagents were weighed in appropriate metal ratios and ground intimately in an agate mortar. The mixtures were pressed into pellets and were calcined at 1173 K. The calcined materials were reground and sintered in air at 1573 K for several days with intermediate regrinding and repelletizing.

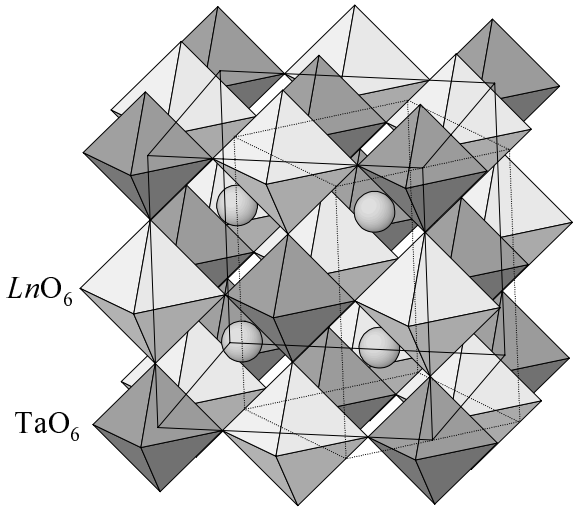

Figure 2. The crystal structure of Ba_2LnTaO_6. The solid and dashed lines indicate the cubic and monoclinic unit cells, respectively.

X-ray diffraction measurements were carried out at room temperature in the range $10^\circ < 2\theta < 120^\circ$ using an angle step of 0.02° with Cu Kα radiation on a MultiFlex diffractometer (Rigaku). The x-ray diffraction patterns were analysed by the Rietveld method, using the program RIETAN2000 [8].

The temperature dependence of magnetic susceptibilities was measured under a zero-field-cooled condition (ZFC) in the temperature range 5–300 K (5–400 K for Sm and Eu compounds) using a SQUID magnetometer (Quantum Design, MPMS-5S). The magnetic field, which was applied after the sample was cooled from 300 K to 5 K in zero field, was 0.1 T.

The ^{151}Eu Mössbauer spectrum was measured with a Mössbauer spectrometer VT-6000 (Laboratory Equipment Co.) in the constant acceleration mode. The spectrometer was calibrated with a spectrum of α-Fe at room temperature. A $^{151}SmF_3$ radiation source (1.85 GBq) was used and the γ-rays were detected with a NaI scintillation counter. EuF_3 was used as a reference standard for the chemical isomer shift. The average surface density of the sample was 14.0 mg (Eu) cm^{-2}. Mössbauer measurements were conducted at 12, 100, 200 and 300 K, using a cryostat system CryoMini (Iwatani Industrial Gases Co.).

3. Results and discussion

3.1. Crystal structures

The results of the x-ray diffraction measurements show that Ba_2LnTaO_6 compounds have a single phase. The x-ray diffraction patterns for Ba_2LnTaO_6 (Ln = Y, Dy–Lu) were indexed with a cubic unit cell, whereas Ln = La, Pr, Nd, Sm–Tb compounds were monoclinically distorted. Figure 1 shows the x-ray diffraction profiles for Ba_2LaTaO_6 and Ba_2LuTaO_6. The diffraction reflection at $2\theta \simeq 18^\circ$ was found for any compound. The presence of this reflection indicates the ordered arrangements between the B site ions. Therefore, it is considered that they have an ordered perovskite-type structure with rock salt sublattice. This structure generally adopts a cubic unit cell (space group: $Fm\bar{3}m$; $2a_p \times 2a_p \times 2a_p$) or a monoclinic one (space group: $P2_1/n$; $\sqrt{2}a_p \times \sqrt{2}a_p \times 2a_p$) [4]. We have performed the Rietveld analysis for the x-ray

diffraction profiles for these compounds, using the program RIETAN2000 [8]. The crystal structure of Ba_2LnTaO_6 is illustrated in figure 2. The crystallographic data for Ba_2LaTaO_6 and Ba_2LuTaO_6 are shown in table 1. The unit cell parameters and the reliability factors for Ba_2LnTaO_6 are listed in table 2.

Table 1. Unit cell parameters and reliability factors for Ba_2LnTaO_6.

Ln	a (Å)	b (Å)	c (Å)	β (°)	R_{wp} (%)	R_I (%)	R_e (%)
Y	8.4368(1)	—	—	—	12.61	1.53	7.86
La	6.1453(2)	6.0946(2)	8.6091(4)	90.335(1)	11.52	1.40	9.08
Pr	6.0919(2)	6.0561(2)	8.5545(2)	90.157(1)	11.62	1.51	9.52
Nd	6.0808(2)	6.0476(2)	8.5425(2)	90.142(1)	11.41	1.40	9.14
Sm	6.0468(3)	6.0225(3)	8.5107(3)	90.038(6)	11.43	1.22	9.08
Eu	6.0191(7)	6.0152(6)	8.4964(2)	90.00(4)	11.50	1.35	9.03
Gd	6.015(3)	6.013(2)	8.4852(2)	90.00(3)	13.80	1.93	7.79
Tb	5.993(3)	5.993(3)	8.4651(1)	90.00(2)	10.80	2.06	7.55
Dy	8.4571(2)	—	—	—	13.34	1.56	8.92
Ho	8.4427(2)	—	—	—	13.57	1.91	8.04
Er	8.4240(1)	—	—	—	12.09	1.44	7.91
Tm	8.4064(1)	—	—	—	11.12	1.47	7.31
Yb	8.3894(1)	—	—	—	11.86	1.20	7.64
Lu	8.3760(1)	—	—	—	12.85	1.49	7.76

Table 2. Structural parameters for Ba_2LnTaO_6 (Ln = La and Lu).

Atom	Site	x	y	z	B (Å^2)
Ba_2LaTaO_6 space group: $P2_1/n$					
Ba	4e	0.002(1)	0.002(1)	0.248(1)	0.55(3)
La	2d	1/2	0	0	0.12(5)
Ta	2c	1/2	0	1/2	0.10(4)
O(1)	4e	0.232(6)	0.279(5)	0.035(7)	1.0(3)
O(2)	4e	0.206(5)	−0.243(5)	0.034(7)	1.0(3)
O(3)	4e	−0.061(3)	0.517(9)	0.224(2)	1.0(3)
Ba_2LuTaO_6 space group: $Fm\bar{3}m$					
Ba	8c	1/4	1/4	1/4	0.58(2)
Lu	4b	1/2	1/2	1/2	0.23(6)
Ta	4a	0	0	0	0.24(6)
O	24e	0.237(1)	0	0	0.8(1)

Figure 3 shows the variation of lattice parameters for Ba_2LnTaO_6 with the ionic radius of Ln^{3+} in the six coordination. The lattice parameters, a_m b_m and c_m (for the monoclinic cell) and a_c (for the cubic cell) increase with the Ln^{3+} ionic radius. In the monoclinic region, the lattice parameter β_m increases and the differences among a_m, b_m and $c_m/\sqrt{2}$ spread with increase of the Ln^{3+} ionic radius. This fact indicates that the crystal structures of Ba_2LnTaO_6 are more distorted from the cubic symmetry as the size of Ln^{3+} ion becomes larger. This agrees with the tendency found in other ordered perovskites, Ba_2LnNbO_6 [9], A_2LnIrO_6 (A = Sr, Ba) [10–12], and Sr_2LnRuO_6 [13].

Figure 4 shows the variation of the average Ln–O and Ta–O bond lengths for the Ba_2LnTaO_6 compounds against the ionic radius of Ln^{3+}. It is found that the average Ln–O bond length increases with the ionic radius of Ln^{3+}, while the average Ta–O bond length is nearly constant (∼1.99 Å). This value is close to the Ta^{5+}–O^{2-} bond length calculated from

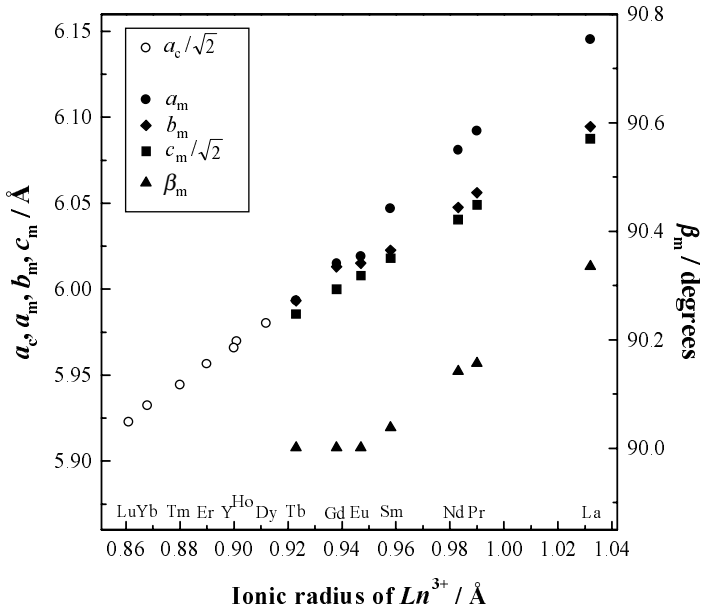

Figure 3. Variation of lattice parameters for Ba_2LnTaO_6 with the ionic radius of Ln^{3+}.

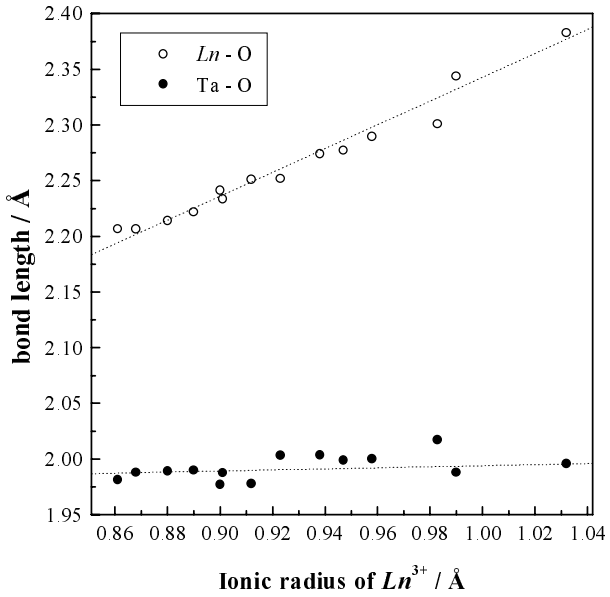

Figure 4. Variation of average bond lengths Ln–O and Ta–O for Ba_2LnTaO_6 with the ionic radius of Ln^{3+}.

Shannon's ionic radii (2.04 Å), rather than the Ta^{4+}–O^{2-} bond length (2.08 Å) [14]. Therefore, it is considered that the tantalum ions in Ba_2LnTaO_6 are in the pentavalent state and all the lanthanide ions are in the trivalent state.

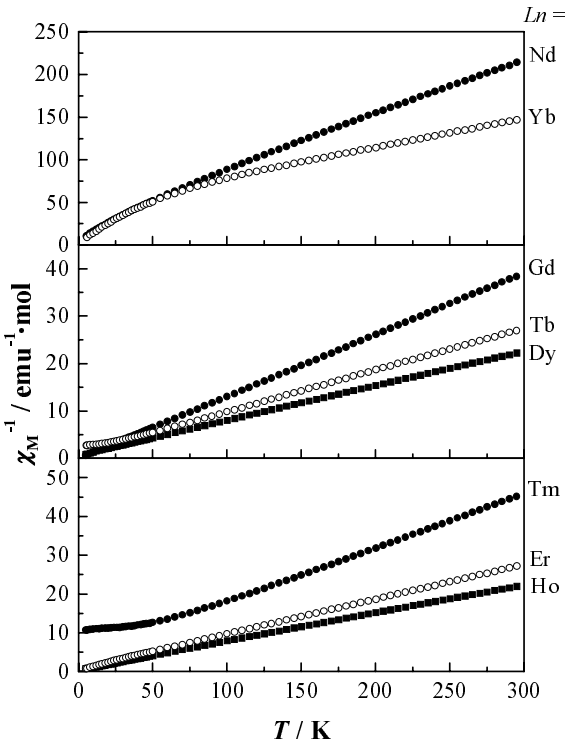

Figure 5. Temperature dependence of the inverse magnetic susceptibilities of Ba_2LnTaO_6 (Ln = Nd, Gd–Yb).

3.2. Magnetic properties

3.2.1. Ba_2LnTaO_6 (Ln = Nd, Gd–Yb). Figure 5 shows the temperature dependence of the inverse magnetic susceptibilities for Ba_2LnTaO_6 (Ln = Nd, Gd–Yb). The Ta^{5+} ions are nonmagnetic; hence only Ln^{3+} ions contribute to the magnetic behaviour of Ba_2LnTaO_6. These compounds are paramagnetic down to 5 K. The susceptibilities were fitted with a Curie–Weiss law in the whole temperature range (for Gd) or in higher temperature ranges (above 50 K for Nd, Tb–Er; above 100 K for Tm). The effective magnetic moments and Weiss constants determined are listed in table 3. The effective magnetic moments are comparable to the values found in Ba_2LnNbO_6 [9]. These values are consistent with the free-ion ones, assuming that $\Delta E \gg k_B T$, where ΔE is the energy difference between the excited and ground states of the electronic multiplet. The Weiss constants are negative except for the Gd compound. This fact may indicate the existence of a Ln^{3+}–Ln^{3+} antiferromagnetic interaction.

At lower temperatures, the susceptibilities of some compounds departed from the Curie–Weiss law. These departures may be due to the crystal field splitting. In the Yb compound, for example, the ground state $^2F_{7/2}$ of Yb^{3+} is split into two doublets (Γ_6 and Γ_7) and one quartet (Γ_8) in the octahedral symmetry. Taira *et al* determined the energy level of this splitting (the ground state is Γ_6; the first excited state is Γ_8 and $E_{\Gamma 8} - E_{\Gamma 6} = 429.7\ \mathrm{cm}^{-1}$; the second excited state is Γ_7 and $E_{\Gamma 7} - E_{\Gamma 6} = 1225.4\ \mathrm{cm}^{-1}$) and the effective magnetic moment 4.41 μ_B from the fitting of the magnetic susceptibilities [7].

Table 3. The calculated magnetic moments for Ln^{3+} (μ_{calc}) and the experimental effective magnetic moments (μ_{exp}) and Weiss constants (Θ) for Ba_2LnTaO_6.

Compounds	μ_{calc} (μ_B)	μ_{exp} (μ_B)	Θ (K)
Ba_2NdTaO_6	3.62	3.21(1)	−19.5(3)
Ba_2GdTaO_6	7.94	7.83(1)	0.37(5)
Ba_2TbTaO_6	9.72	9.49(1)	−10.3(2)
Ba_2DyTaO_6	10.63	10.26(1)	−6.68(6)
Ba_2HoTaO_6	10.58	10.17(1)	−3.73(12)
Ba_2ErTaO_6	9.59	9.44(1)	−7.73(5)
Ba_2TmTaO_6	7.55	7.83(2)	−35.7(6)

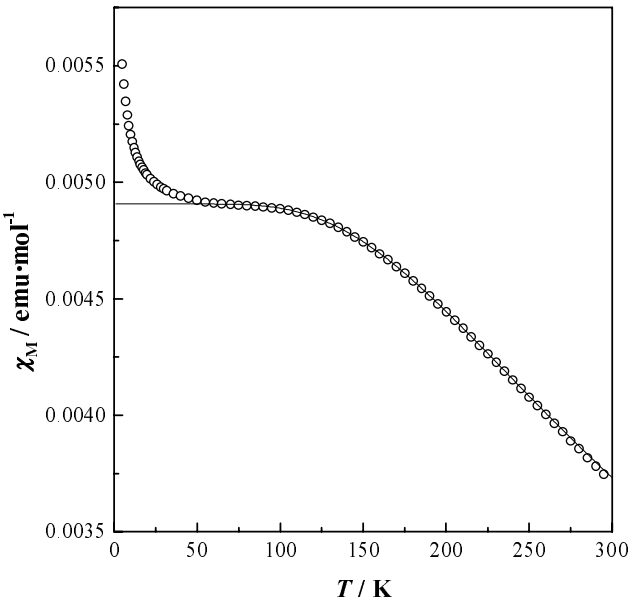

Figure 6. Temperature dependence of the magnetic susceptibility of Ba_2PrTaO_6. A solid line is calculated with equation (1).

3.2.2. Ba_2PrTaO_6. Figure 6 shows the temperature dependence of the magnetic susceptibility measured for Ba_2PrTaO_6. This compound is paramagnetic down to 5 K. The ground state $^3H_4$ of the Pr^{3+} ion is split into one singlet (Γ_1), one doublet (Γ_3) and two triplets (Γ_4 and Γ_5) in the octahedral symmetry. We expect that the ground state and the first excited state are Γ_1 and Γ_4, respectively and that the upper excited states are Γ_3 and Γ_5, which is analogous with the results for $Cs_2NaPrBr_6$ [15]. The wave functions of these states are given by Lea *et al* [16]. In order to explain the temperature dependence of the magnetic susceptibility, we use these wave functions as a first approximation, although the crystal structure of Ba_2PrTaO_6 is distorted from the cubic symmetry to some extent. The magnetic susceptibility of the Pr^{3+} ion is calculated by the Van Vleck equation [17]:

$$\chi(\mathrm{Pr}^{3+}) = \frac{N_A g_J^2 \mu_B^2 J(J+1)}{3k_B T} F(T) \tag{1}$$

where

$$F(T) = \left[3\,\mathrm{e}^{-\Delta_{41}/k_BT} + 75\,\mathrm{e}^{-\Delta_{51}/k_BT} + \frac{80k_BT}{\Delta_{41}}(1-\mathrm{e}^{-\Delta_{41}/k_BT}) + \frac{112k_BT}{\Delta_{41}-\Delta_{31}}(\mathrm{e}^{-\Delta_{31}/k_BT}-\mathrm{e}^{-\Delta_{41}/k_BT}) + \frac{42k_BT}{\Delta_{51}-\Delta_{41}}(\mathrm{e}^{-\Delta_{41}/k_BT}-\mathrm{e}^{-\Delta_{51}/k_BT}) + \frac{48k_BT}{\Delta_{51}-\Delta_{31}}(\mathrm{e}^{-\Delta_{31}/k_BT}-\mathrm{e}^{-\Delta_{41}/k_BT})\right] \times [40(1+2\,\mathrm{e}^{-\Delta_{31}/k_BT}+3\,\mathrm{e}^{-\Delta_{41}/k_BT}+3\,\mathrm{e}^{-\Delta_{51}/k_BT})]^{-1}$$

and N_A, μ_B and k_B are Avogadro number, Bohr magneton and Boltzmann constant, respectively. Δ_{31}, Δ_{41} and Δ_{51} are the energies of Γ_3, Γ_4 and Γ_5 states above the ground state (Γ_1), respectively. By fitting this equation to the experimental magnetic susceptibility over the temperature range 50–300 K, the effective magnetic moment for Ba_2PrTaO_6 was obtained to be 3.4 μ_B. This value is close to the free-ion value (3.58 μ_B). The estimated energy levels are $\Delta_{41} = 459\ \mathrm{cm}^{-1}$, $\Delta_{51} \simeq 1600\ \mathrm{cm}^{-1}$ and $\Delta_{31} \simeq 1800\ \mathrm{cm}^{-1}$. The fitting curve is shown in figure 6. The increase in the susceptibility at low temperatures may be due to the existence of the paramagnetic Ta^{4+} ion derived from a slight oxygen deficiency.

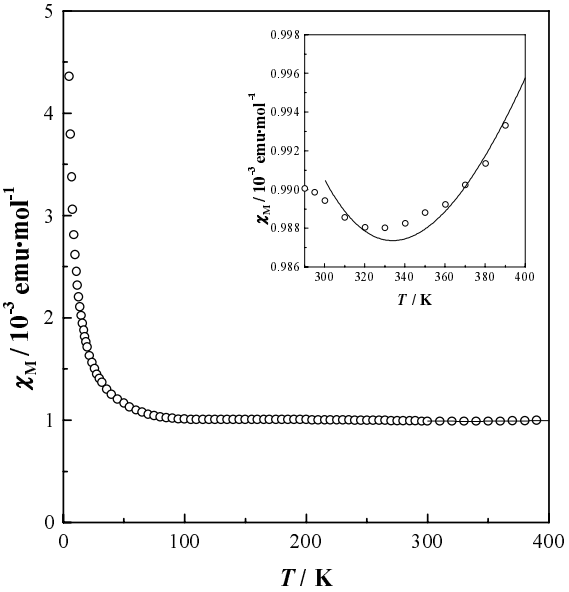

Figure 7. Temperature dependence of the magnetic susceptibility of Ba_2SmTaO_6. A solid line is calculated with equation (2) in the temperature range of 300–400 K.

3.2.3. Ba_2SmTaO_6. The temperature dependence of the magnetic susceptibility for Ba_2SmTaO_6 is shown in figure 7. The ground state of the Sm^{3+} ion is $^6H_{5/2}$. At low temperatures, only this magnetic $^6H_{5/2}$ ground multiplet is populated. However, the energy difference between the ground state ($^6H_{5/2}$) and the first excited state ($^6H_{7/2}$) is not very large compared with k_BT. Hence, we must take the population to the excited state into consideration in the calculation of magnetic susceptibility at higher temperature (300–400 K).

The temperature dependence of the susceptibility is given by [18],

$$\chi(\mathrm{Sm}^{3+}) = \frac{C_1}{T} + \alpha_1 + \frac{C_2}{T}\,\mathrm{e}^{-\Delta/T} \tag{2}$$

where Δ is the energy difference between the ground state and the first excited state, and C_i and α_1 are the Curie and Van Vleck constant, respectively. Δ and α_1 are not independent since $\alpha_1 = 1.07/\Delta$, if Δ is given in Kelvin. C_2 is fixed at 1.34 emu K mol^{-1}, which is calculated for the first excited state $^6H_{7/2}$. The fit to the experimental data gives $C_1 = 0.0588$ emu K mol^{-1} and $\Delta = 1005$ cm^{-1}. The effective magnetic moment for the ground state is 0.69 μ_B, and is smaller than the free-ion moment (0.845 μ_B), which is probably due to the effect of the crystal field. The obtained spin–orbit coupling constant λ is 287 cm^{-1}.

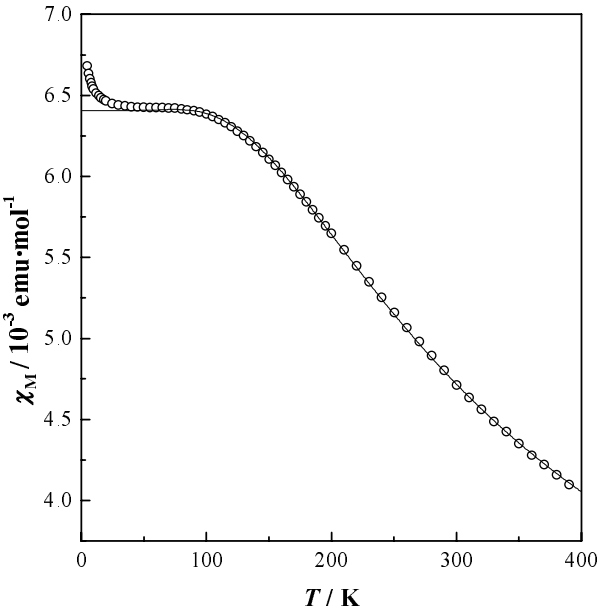

Figure 8. Temperature dependence of the magnetic susceptibility of Ba_2EuTaO_6. A solid line is calculated with equation (3).

3.2.4. Ba_2EuTaO_6. Figure 8 shows the temperature dependence of the magnetic susceptibility for Ba_2EuTaO_6. The susceptibility increases with decreasing temperature down to ~100 K; below this temperature it flattens out. At lower temperatures (<20 K) it increases again. This feature may indicate a small quantity of paramagnetic Ta^{4+} ion, which is similar to the case of Ba_2PrTaO_6. Below 100 K only the non-magnetic ground state ($^7F_0$) is populated, and the susceptibility plateau is due to the temperature-independent term of the Van Vleck formula. The molar magnetic susceptibility for Eu^{3+} taking into account the contribution from the excited states ^7F_J ($J = 1, 2, \ldots, 6$) can be written by the following equation [17],

$$\chi(\mathrm{Eu}^{3+}) = \frac{N_A\mu_B^2}{3k_B\gamma T}\,\frac{24 + (13.5\gamma - 1.5)\,\mathrm{e}^{-\gamma} + (67.5\gamma - 2.5)\,\mathrm{e}^{-3\gamma} + (189\gamma - 3.5)\,\mathrm{e}^{-6\gamma} + \cdots}{1 + 3\,\mathrm{e}^{-\gamma} + 5\,\mathrm{e}^{-3\gamma} + 7\,\mathrm{e}^{-6\gamma} + \cdots} \tag{3}$$

where $\gamma = /k_BT$ is 1/21 of the ratio of the overall multiplet width to k_BT. By fitting this equation to the experimental magnetic susceptibility above 50 K, the spin–orbit coupling

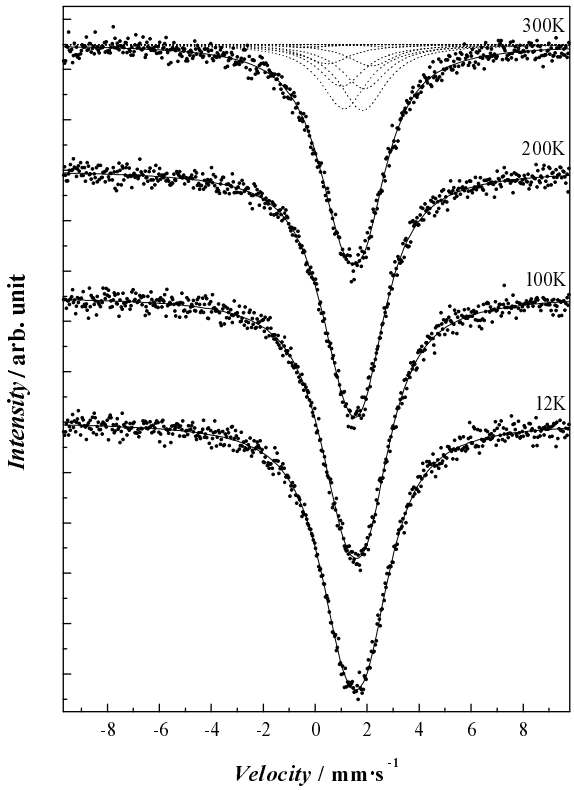

Figure 9. ^{151}Eu Mössbauer spectra of Ba_2EuTaO_6 at 12, 100, 200 and 300 K.

constant λ was obtained to be 332 cm^{-1}. This value is close to the values reported in other ordered perovskites, for example, 339 cm^{-1} (Ba_2EuNbO_6) [9] and 364 cm^{-1} (Ba_2EuIrO_6) [12].

3.3. ^{151}*Eu Mössbauer spectrum*

^{151}Eu Mössbauer spectra for Ba_2EuTaO_6 measured at 12, 100, 200 and 300 K are shown in figure 9. Because of the low symmetry of the europium site in Ba_2EuTaO_6 (point symmetry: $\bar{1}$), an electric field gradient tensor should exist at this site. The quadrupole Hamiltonian is given by

$$H_{\text{quad}} = \frac{e^2 q Q}{4I(2I-1)}[3I_z^2 - I(I+1) + \eta(I_x^2 - I_y^2)] \tag{4}$$

where Q is the quadrupole moment, I is the nuclear spin, $eq = V_{zz}$ and $\eta = (V_{xx} - V_{yy})/V_{zz}$ (V_{ii} is the electric field gradient tensor). The asymmetry parameter η is not equal to zero, because the symmetry at the Eu site is not axially symmetric. Then, the 12 possible transitions (eight allowed transitions and four forbidden transitions) due to a quadrupole interaction were taken into account; the observed data were fitted with the sum of these Lorenzian lines. In order to derive these Lorenzian equations, the results by Shenoy and Dunlap [19] were used and the ratio of the excited and ground state quadrupole moments ($R_Q = Q_e/Q_g$) was taken as 1.312 [20]. Therefore, the fitting parameters are isomer shift (δ), quadrupole coupling constant ($eV_{zz}Q_g$), asymmetry parameter (η) and two common parameters for 12 Lorenzians, i.e., linewidth (Γ) and peak intensity (I_0).

Table 4. Mössbauer spectrum parameters for Ba_2EuTaO_6.

T (K)	δ (mm s^{-1})	$eV_{zz}Q_g$ (mm s^{-1})	η	Γ (mm s^{-1})	I_0 (%)
300	1.441(10)	5.2(3)	0.76(10)	2.15(7)	10.6(2)
200	1.466(8)	4.6(3)	0.60(13)	2.25(6)	11.3(2)
100	1.532(8)	5.3(2)	0.79(8)	2.21(6)	12.7(2)
12	1.536(8)	5.1(3)	0.93(8)	2.21(6)	12.9(2)

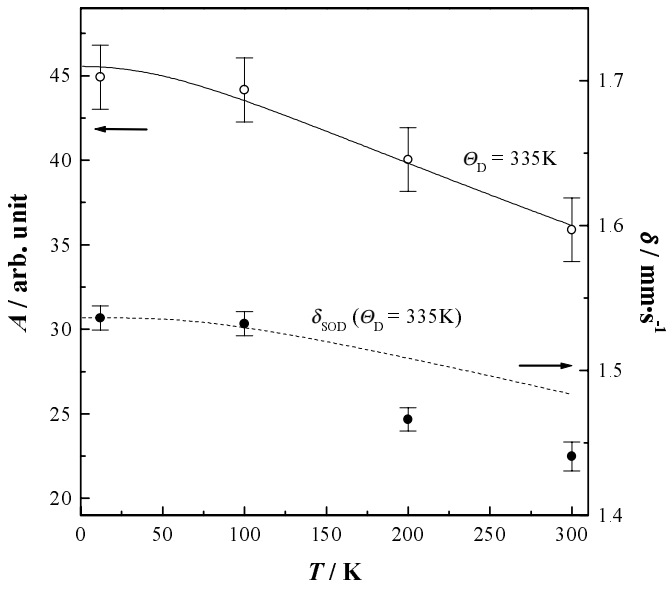

Figure 10. Temperature dependence of absorption area of intensity curves (A) and the isomer shift (δ) of Ba_2EuTaO_6. The solid line is the theoretical curve of the recoil-free fraction (equation (5); $\Theta_D = 335$ K) normalized to A; a broken line is the theoretical curve of the second-order Doppler shift with $\Theta_D = 335$ K (equation (6)).

The calculated spectra are shown in figure 9, and the obtained fitting parameters are listed in table 4. The isomer shifts are 1.441–1.536 mm s^{-1}, which confirms that the europium ions are in the trivalent state. The quadrupole coupling constants and asymmetry parameters were determined to be 4.6–5.3 mm s^{-1} and 0.60–0.93, respectively. This fact indicates the existence of the electric field gradient at the Eu nuclei. The sign of $eV_{zz}Q_g$ is positive in this case, which is the same result as those for other analogous compounds measured at room temperature: 4.96 mm s^{-1} for Ba_2EuNbO_6 [9] and 4.92 mm s^{-1} for Ba_2EuIrO_6 [12].

Figure 10 shows the temperature dependence of the absorption area of the intensity curves (A) and isomer shifts (δ). The area of the intensity is proportional to the recoil-free fraction f. The recoil-free fraction is represented by the following equation [21]:

$$f = \exp\left[\frac{-6E_R}{k_B\Theta_D}\left\{\frac{1}{4} + \left(\frac{T}{\Theta_D}\right)^2 \int_0^{\Theta_D/T} \frac{x\,\mathrm{d}x}{(\mathrm{e}^x - 1)}\right\}\right] \tag{5}$$

where Θ_D is the Debye temperature, and E_R is the free-atom recoil energy. The theoretical curve with $\Theta_D = 335$ K (the solid line in figure 10) is in good agreement with the experimental data. The isomer shift decreases with increasing temperature. This decrease must be due to the second-order Doppler shift and the change in the electron density at the Eu nuclei. According

to the Debye model, the temperature dependence of the second-order Doppler shift ($\Delta\delta_{SOD}$) can be expressed by the following equation [22]:

$$\Delta\delta_{SOD} = \frac{-9k_BT}{2Mc}\left\{\frac{1}{8}\frac{\Theta_D}{T} + \left(\frac{T}{\Theta_D}\right)^3 \int_0^{\Theta_D/T} \frac{x^3\,\mathrm{d}x}{(\mathrm{e}^x - 1)}\right\} \tag{6}$$

where M and c are the mass of the isotope and the speed of light, respectively. The temperature dependence of $\Delta\delta_{SOD}$ ($\Theta_D = 335$ K) is calculated using this equation and it is shown in figure 10 (the broken line). The difference in the isomer shifts between 12 and 300 K (0.096 mm s^{-1}) is larger than that in the second-order Doppler shifts (0.053 mm s^{-1}). This difference is probably attributable to the decrease of the electron densities at the Eu nuclei caused by the increase of Eu–O bond length [23, 24]. This increase may be derived from the thermal expansion of the lattice.

Acknowledgments

This work was supported by the Iwatani Naoji Foundation's research grant and by a Grant-in-Aid for Scientific Research on Priority Area 'Novel quantum phenomena in transition metal oxides–spin–change–orbital coupled systems' No 12046203 from the Ministry of Education, Science, Sports and Culture of Japan. One of the authors (YD) thanks the Research Fellowships of the Japan Society for the Promotion of Science for Young Scientists.

References

[1] Patterson F K, Moeller C W and Ward R 1963 *Inorg. Chem.* **2** 196
[2] Brandle C D and Steinfink H 1971 *Inorg. Chem.* **10** 922
[3] Brusset H, Giller-Pandraud M H and Rajaonera P 1975 *Mater. Res. Bull.* **10** 209
[4] Anderson M T, Goodenough J B, Taylor G A and Poeppelmeier K R 1993 *Prog. Solid State Chem.* **22** 197
[5] Filip'ev V S and Fesenko E G 1961 *Kristallografiya* **6** 770
[6] Galasso F S, Layden G K and Flinchbaugh D E 1966 *J. Chem. Phys.* **44** 2703
[7] Taira N and Hinatsu Y 2000 *J. Solid State Chem.* **150** 31
[8] Izumi F and Ikeda T 2000 *Mater. Sci. Forum* **321–324** 198
[9] Henmi K and Hinatsu Y 1999 *J. Solid State Chem.* **148** 353
[10] Harada D, Wakeshima M and Hinatsu Y 1999 *J. Solid State Chem.* **145** 356
[11] Wakeshima M, Harada D, Hinatsu Y and Masaki N 1999 *J. Solid State Chem.* **147** 618
[12] Wakeshima M, Harada D and Hinatsu Y 2000 *J. Mater. Chem.* **10** 419
[13] Doi Y and Hinatsu Y 1999 *J. Phys.: Condens. Matter* **11** 4813
[14] Shannon R D 1976 *Acta Crystallogr.* A **32** 751
[15] Furrer A and Güdel H 1997 *Phys. Rev.* B **56** 15 062
[16] Lea K R, Leask M J M and Wolf W P 1962 *J. Phys. Chem. Solids* **23** 1381
[17] Van Vleck J H 1932 *The Theory of Electric and Magnetic Susceptibilities* (Oxford: Clarendon)
[18] Goya C F, Mercader R C, Causa M T and Tovar M 1996 *J. Phys.: Condens. Matter* **8** 8607
[19] Shenoy G K and Dunlap B D 1969 *Nucl. Instrum. Methods* **71** 285
[20] Stevens J G 1981 *Handbook of Spectroscopy* ed J W Robinson vol III (Boca Raton, FL: Chemical Rubber Company) p 464
[21] Mahesh K 1974 *Phys. Status Solidi* b **61** 695
[22] Housley R M and Hess F 1996 *Phys. Rev.* **146** 517
[23] Tanabe S, Hirao K and Soga N 1989 *J. Non-Cryst. Solids* **113** 178
[24] Nakamura A, Masaki N M, Nakada M, Saeki M, Tomimoto K and Akimitsu J 1996 *Ceram. Trans.* **71** 295